International Journal of Microwave and Wireless Technologies

cambridge.org/mrf

On the efficient computation of range and Doppler data in noise radar

Christoph Wasserzier[1,2] and Gaspare Galati[1,3]

[1]Tor Vergata University, via del Politecnico 1, Rome, Italy; [2]Fraunhofer Institute for High Frequency Physics and Radar Techniques FHR, Fraunhoferstr. 20, 53343 Wachtberg, Germany and [3]CNIT, National Inter-University Consortium for Telecommunications

Research Paper

Cite this article: Wasserzier C, Galati G (2019). On the efficient computation of range and Doppler data in noise radar. *International Journal of Microwave and Wireless Technologies* **11**, 584–592. https://doi.org/10.1017/S175907871800171X

Received: 21 September 2018
Revised: 4 December 2018
Accepted: 7 December 2018
First published online: 4 February 2019

Keywords:
Noise radar technology; range filter bank; range-doppler map; moving target detection

Author for correspondence: Christoph Wasserzier christoph.wasserzier@fhr.fraunhofer.de

Abstract

In noise radar, digital signal processing algorithms for implementing the computation of the Cross Ambiguity Function through range correlation and Doppler compensation call for optimized solutions. In fact, to achieve a high coherent processing gain, they often compute a large amount of data beyond the maximum range and/or the maximum radial velocity of interest, adding useless information. A novel, efficient algorithm, called Range Filter Bank, is proposed to implement a scope-tailored computation of range/Doppler data in continuous emission noise radar. Downstream its theoretical analysis, the algorithm has been applied to a real-life case study based on dedicated field experiments, in which good quality kinematic data of a car moving at various speeds have been extracted.

Introduction

Active research is being carried out worldwide on Noise Radar Technology (NRT), i.e. on the use of random (more precisely, pseudo-random in today's digital generation and processing systems) waveforms for many radar applications, mostly at short range. The main reasons for investigating these radar waveforms are threefold:

a) robustness against mutual interference [1,2]
b) low probability of intercept [3]
c) controllable ambiguity levels, both in range and in radial velocity (Doppler frequency) [4]

This paper is focused on item (c) and considers the case of continuous emission (CE) noise radar, i.e. the stochastic counterpart of a continuous-wave (CW) radar, whose frequency-modulated version (FMCW) is probably the most popular one. Generalized, the findings can be used for processing continuously-emitted radar signals such as (pseudo-)noise or orthogonal frequency division multiplex signals. The latter waveform is used in different applications such as Passive Coherent Location (PCL) [5], Multiple Input Multiple Output (MIMO) radars [6] and others.

In order to extract a known signal from a white disturbance background, the matched filter theory leads to computation of the Ambiguity Function (AF) defined in [7], i.e. the correlation of a signal having complex envelope $s(t)$ with its Doppler-shifted (of entity f_D) replica,

$$X(t, f_D) = \int_{-\infty}^{\infty} s(\tau) g^*(t+\tau)\, e^{-j2\pi f_D \tau} d\tau. \quad (1)$$

Operationally, a radar receiver/processor performs the cross-correlation of a Doppler-shifted copy of the transmitted signal and the received signal (over a finite integration time) for a set of Doppler values of interest. This procedure is often called computation of the Cross Ambiguity Function (CAF). Conversely, in the radar waveform design phase [8], the AF is used to quantify the level of unwanted signals (due to ambiguities as well as to side lobes) after matched filtering of the radar echo. In principle, the radar designer would ask for radar waveforms with their AF in shape of a thumbtack (i.e. one with neither ambiguities nor side lobes); a wideband, long duration noise may approximate this behavior. In fact, when both the duration T and the bandwidth B of a radar signal with noise characteristic go to infinity, its AF obviously converges to a bi-dimensional Delta function. However, in the real world both B and T are finite; in particular, B is limited (often, to a few hundred MHz) by the regulations on the use of the electromagnetic spectrum. For example, all on-board civil marine radars have to radiate in the 9300–9500 MHz interval for the X-band, and 2900–3100 MHz for the S-band, i.e. always with $B < 200$ MHz.

Less straightforward are the bounds on T. Here, we consider short/medium range, medium/high-resolution surveillance radar applications, where target data have to be updated at the

© Cambridge University Press and the European Microwave Association 2019

CAMBRIDGE UNIVERSITY PRESS

typical rate going from one second to a few seconds. Below this scan time scale, there are two more time scales, i.e. slow (sweep) time and fast (pulse) time. A radar sweep has a typical duration called *pulse repetition interval* or T_{PRI}, of the rough order of magnitude around hundreds of microseconds, and contains some thousands of range resolution cells, each with duration around 1/B, i.e. often in the order of hundreds of nanoseconds (fast time scale).

In classical *deterministic*, monostatic surveillance radars, the pulse (or more generally, waveform) repetition interval, once defined by setting the instrumented range, has zero or little variations, as well as the scan rate of the antenna. Hence, in those applications, there is very limited flexibility in setting the values of slow and fast time, and, for a given radar wavelength λ, the maximum unambiguous range and radial velocity, R_{max} and $|v_{max}|$, are fixed by the well-known relationships

$$R_{max} = \frac{cT_{PRI}}{2} \tag{2}$$

and

$$v_{max} = \frac{\lambda}{4T_{PRI}} \tag{3}$$

leading to the Range Velocity Product

$$RVP = c \cdot \frac{\lambda}{8} \tag{4}$$

independent of the pulse repetition interval.

But such a situation, which is strictly connected to the signal being periodic, does change when noise radar, with separated transmitting and receiving antennas, continuously transmits a random, hence, aperiodic, waveform. In this case, the concept of sweep has to be reviewed and the most relevant time interval is the one dictated by the dwell time T_D. It is defined as the maximum time interval in which a fixed point-target continuously supplies useful echoes.

When a classic, horizontally scanning antenna for bi-dimensional (2D) radar surveillance is considered, the dwell time is computed by dividing the antenna beam width by the antenna rotation velocity. The order of magnitude of T_D in 2D short-medium range surveillance is often tens of milliseconds, and in each scan the information content that can be extracted by an individual target is proportional (for both deterministic and noise radars) to the ratio between the dwell time and the signal's sampling period.

For a staring, or persistent, radar the scan is absent and the dwell time is limited by the transit time, in a range resolution cell, of the target having radial velocity v_r, i.e. T_D is less than $(c/(2Bv_r))$, leading to a possibly large value (order of millions) of the theoretical number of independent signal samples, i.e. up to $(c/(2v_r))$.

In typical applications, with a signal sampling period $T_S = k/B$ (with the oversampling factor k being of the order of the unity) the number of digital samples to be processed in an ideal computation of the full CAF is equal to $k \cdot B \cdot T_D$, i.e. often reaches the impractical order of millions, calling for separation of the range and Doppler processing.

This separation is relatively straightforward when the radar waveform is repetitive (i.e. in the deterministic case). In fact, in this case, T_D includes a given number N_S of sweeps (i.e. $T_D = N_S \cdot T_{PRI}$), and the fast time processing, aimed to the extraction of range data, is done in each of them. The fast time processing is normally followed by re-organization of the processed data (sometimes called corner turn) and by the slow time processing, aimed to provide a further processing gain and to extract Doppler (i.e. radial velocity) data.

Note that, regardless of the waveform type (deterministic or random), the separation of range extraction from Doppler (i.e. radial velocity) extraction calls for choosing the duration T_W of the transmitted waveform. Compatibly with the power budget, T_W has to be short enough to have a negligible, or at least acceptable, Doppler sensitivity. This means that, denoting f_{max} the maximum Doppler frequency, the condition shall held that $T_W \cdot f_{max} << 2\pi$. A practical rule may be to keep, for both deterministic and random waveforms, the product $T_W \cdot f_{max}$ less than a small fraction (e.g. 1/8) of the complete phase rotation:

$$T_W \cdot f_{max} < \frac{\pi}{4} \tag{5}$$

Based on these considerations adequate Doppler compensation is required in many noise radar applications.

This compensation is often implemented by calculating the well-known range–Doppler map [9], representing a set of Doppler-compensated range profiles. Usually, in NRT this is performed by computing, by means of fast algorithms, the CAF [10,11] as explained above. Approaches for efficient range–Doppler processing in CE and CW radars are strongly needed, as the calculation of the CAF is inefficient in most cases [4]. Besides the CAF approach, an optimized algorithm for digitally analyzing the Doppler signal in a smaller number of range cells has been published in [12]. In the manner similar to the one of Doppler analysis in FMCW radars, [13] describes an algorithm that is based on partitioning the reference signal into batches.

Let us summarize the key points in the processing system proposed here: in a CE noise radar, waveforms are not repetitive, leaving freedom to choose the duration of the fast time and of the slow time processing intervals, within the finite and fixed T_D.

This paper presents a novel procedure resulting in fully customizable range–Doppler maps in CE noise radar. The advantages of this Range Filter Bank (RFB) algorithm over the CAF in computational cost have been briefly presented in [4]. In the following, a detailed description of the procedure of the RFB is given, which shows how the RFB overcomes range-dependent correlation losses and offers tailored range–Doppler computations with minimum overhead. Verification of the RFB algorithm is shown based on the results of dedicated field experiments implemented thanks to a working noise radar demonstrator in order to evaluate the practical performance and effectiveness of the proposed algorithm.

The RFB algorithm

In the following, two major problems of noise radar signal processing are addressed and suggested solutions are presented. Each of these problems depends on the considered dimension of the range–Doppler analysis. First, the range-related techniques are presented and afterwards a Doppler-related algorithmic procedure is introduced. The two-phase characteristics of the RFB algorithm are finally highlighted.

The RFB method is based on the fact that the CE of a noise-radar grants a peculiar flexibility to be exploited by dividing the

https://doi.org/10.1017/S175907871800171X Published online by Cambridge University Press

received signal into a (well greater than the unity) number P of processing segments, each with a fixed, convenient duration T_r. Hence:

$$T_D = PT_r. \tag{6}$$

As all P noise signal segments are stochastically independent, any subset of M out of P segments can be used for range-scope enlargement. A strict requirement for the usage of the RFB is that the waveform is non-repetitive during the analysis, i.e.

$$T_W \geq PT_r. \tag{7}$$

Algorithmic details of the RFB in range domain

This section focuses on range calculations only. It describes a common problem in noise radar signal processing as well as a Filter Bank approach to overcome this problem. The main design parameters and criteria of the presented algorithm are explained in detail.

The range limitation problem

A current problem in radar signal processing often occurs when digital correlation is applied for range measurement: digital correlation often produces an inefficiently high amount of range calculations for a given range region of interest (ROI) as shown in the following.

The received echo signal $s(t)$ of a single target in range R is a delayed, possibly Doppler shifted and disturbed version of the transmitted radar waveform $g(t)$. It is

$$s(t) = Ag(t - \tau_R)e^{j2\pi f_D t} + n(t), \tag{8}$$

where f_D denotes the Doppler shift, $n(t)$ represents the additive disturbances and $\tau_R = ((2R)/c)$ is the round-trip delay as defined by the target range R. The value of the amplitude A depends on several factors including distance and reflectivity of the target.

The cross-correlation function $R_{sg}(\tau)$ in general measures the similarity of two signals $s(t)$ and $g(t)$ in dependency of their relative delay τ [14].

$$R_{sg}(\tau) = \int_{-\infty}^{\infty} s(t)g^*(t - \tau)dt. \tag{9}$$

Often (9) is utilized for measuring the target distance in radar applications, as R_{sg} has its maximum value for $\tau = \tau_R$ when (8) is taken into account. The cross-correlation function $R_{sg}(\tau)$ of two continuous-time signals $s(t)$ and $g(t)$ can only be computed by dividing them into a finite number of segments of duration T_r and computing their linear convolution. This is usually done through the circular convolution, effectively computed in the frequency domain by multiplication of the relevant spectra followed by inverse Fourier transform.

The value of the peak amplitude of $|R_{sg}(\tau)|$ depends on the delay τ_R of the echo signal $s(t)$ proportional to $g(t - \tau_R)$ and the computation is affected by the finite length T_r of the correlation process and the non-periodic structure of the noise waveform. In case of a noise waveform with a rectangular window, this peak value for different round-trip delays τ_R follows a triangular shape defined by the section length T_r. The triangular function

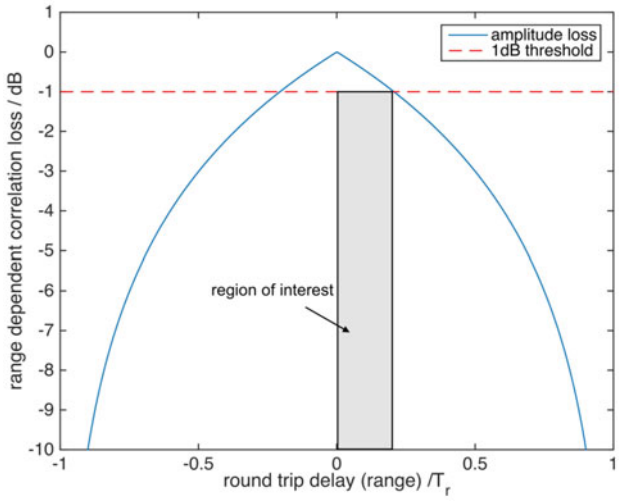


Fig. 1. Range-dependent loss: due to linear decline of the correlation peak, a range scope much higher than the range region of interest needs to be computed in direct range correlation. In this example, a radar application with a tolerable loss of 1dB in its range correlation amplitude is drawn. The target round trip delay then is $\tau_{1dB} \leq ((T_r)/5)$ for a given correlation interval of length T_r. This restriction will be eliminated later in this paper.

reaches its maximum value for $\tau_R = 0$. It then linearly declines to zero for target delays $\tau_R = T_r$ and $\tau_R = -T_r$. Hence, the absolute maximum target range, which can be processed, is limited by the correlation length T_r. Beyond this, practical radar applications might only cope with a correlation loss, say, of 1 dB leading to a much shorter acceptable target distance having a maximum round-trip delay of $\tau_{1dB} \leq ((T_r)/5)$. The described standard range-correlation procedure calculates the full range scope of $((cT_r)/2)$ although 4/5 of the range profile correspond to ranges beyond the ROI. This is quite inefficient as illustrated in Fig. 1 with logarithmic representation of the linear range-dependent correlation loss. The inefficiency is removed in the novel filter bank approach described hereafter.

Usage of a bank of matched filters

A novel approach of overcoming the above-said limitation makes use of the aperiodic characteristic of the radar waveform and also of the fact that, in principle, the instantaneous bandwidth B of any section of a continuous noise signal does not depend on the section length.

In this algorithm, the previously described range-dependent amplitude loss in the correlation signal is compensated for by coherently combining a number of suitable range sectors. This procedure is illustrated in Fig. 2 and can be performed in two steps.

The first step corresponds to the filter bank composition and simultaneous filter operations which are highlighted by a gray box in Fig. 2. In this step, M range correlations of the same echo signal section $s(t)$ with different properly delayed reference signals $g_m(t)$ are computed. The signals $g_m(t)$, which are defined as

$$g_m(t) = g(t - mT_r) \cdot \mathrm{rect}\left(\frac{t}{T_r}\right), \quad m = 0, 1, \ldots, (M-1) \tag{10}$$

form a Range-Filter Bank. Each element of the filter bank represents a particular past section of the known transmitted signal $g(t)$

https://doi.org/10.1017/S175907871800171X Published online by Cambridge University Press

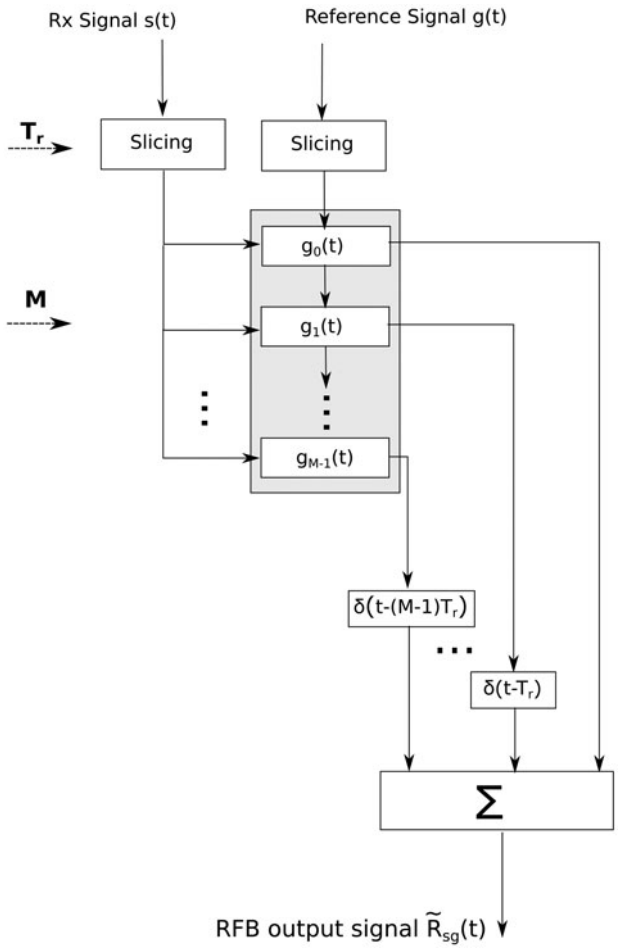


Fig. 2. The Range Filter Bank core algorithm for efficient computation of range profiles. The design parameter T_r which represents the length of each elementary matched filter operation defines the update rate of the resulting extended range profiles. The design parameter M describes the number of matched filters in the filter bank and thus it defines the range scope according to (12).

with all elements having length T_r. According to (9) and (10) the resulting correlations R_{sg_m} in each stage of the filter bank have a length of $2T_r$ as both, positive and negative delay values are taken into account.

In a second step the resulting range profiles of all M channels of the filter bank are subsequently combined to create a single range profile $\tilde{R}_{sg}$. This profile is formed by summing appropriately delayed range sections R_{sg_m} to

$$\tilde{R}_{sg}(t) = \sum_{m=0}^{M-1} R_{sg_m}(t - mT_r). \tag{11}$$

The M delay blocks in (11), each of which has an impulse response of $\delta(t - mT_r)$, produce a 50% overlap of each of the adjacent range correlations causing a pairwise compensation of the triangular-shaped amplitude characteristic, that each single range correlation R_{sg_m} has.

The resulting signal $\tilde{R}_{sg}$ has a length corresponding to a round-trip delay of $(M+1)\cdot T_r$ whereas the maximum computed range of targets with fully restored correlation amplitude is enhanced to

$$R_{max} = \frac{c}{2}\cdot(M-1)\cdot T_r. \tag{12}$$

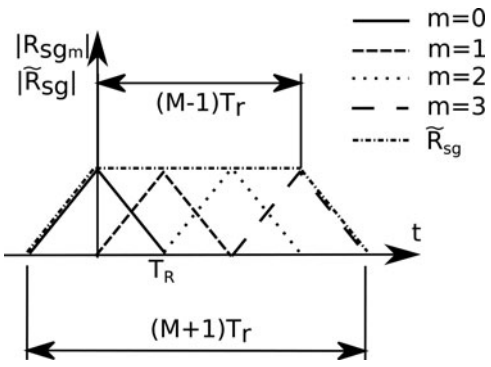


Fig. 3. Range-dependent loss compensation performed by a Range Filter Bank with M=4 elements. In the middle section an amplitude plateau of $\tilde{R}_{sg}$ spanning a length of $(M-1)T_r$ can be observed.

Figure 3 demonstrates the RFB principle of adding overlapping range sectors for an exemplary value of M=4.

The first phase of the RFB algorithm produces a sequence of range profiles with a range profile update rate that is independent from the range scope corresponding to a much higher measurable round-trip delay of $(M-1)\cdot T_r$ for $M>2$. The efficiency of the range calculation is defined by the design parameter M which corresponds to the number of filters in the filter bank. The parameter M defines the ratio of the range of interest to the computed range scope (maximum range), i.e. to the instrumented radar range.

The second design parameter is the length of each matched filter T_r. The higher the design parameter M is chosen, the shorter the section length T_r becomes for a given instrumented range. A smaller value of T_r leads to a high range profile update rate but lowers the elementary processing gain. Let us recall that, in principle, the theoretical maximum coherent processing gain in the CAF computation is bound to $B\cdot T_D$. Using the RFB a large overall range scope is covered by (12) but the processing gain of this operation is defined by a single slice length and thus is equal to the time-bandwidth product of a single elementary filter bank operation of only

$$G_{corr} = B\cdot T_r. \tag{13}$$

Ways to improve the processing gain of the RFB without lowering the range profile update rate and exploiting P outputs are explained in the following.

Application of the RFB in the Doppler domain

This section describes how the correlation gain of the RFB processing can be increased. An approach for range–Doppler calculations is presented offering range scope and maximum unambiguous Doppler frequency which are independently selectable.

The starting point of the proposed gain enhancement procedure is formed by a set of P adjacent (i.e. in the *slow time* domain, equivalent to the sweeps-azimuth domain in classical 2D surveillance radar) extended range profiles which have been created by the bank of matched filters as shown in Fig. 2. In order to enhance the signal to noise ratio (SNR) of target echoes in the output signal of (11), coherent processing of this series of range profiles is performed. The over-all processing gain, then, is P-fold increased from (13) to

$$G_{RFB} = B\cdot(P\cdot T_r). \tag{14}$$

https://doi.org/10.1017/S175907871800171X Published online by Cambridge University Press

The bonded range scope and Doppler ambiguity problem

In conventional radars, as described in the introduction, the pulse repetition interval (T_{PRI}) defines the unambiguous range and also the extent and resolution of the Doppler analysis: long T_{PRI} values lead to large unambiguous range but short unambiguous Doppler interval. The opposite is true for short T_{PRI} values.

In a manner similar to the FMCW Doppler analysis, [13] describes an algorithm which is based on sectioning of the reference signal in the so-called *batches* of length T_B. These batches are processed in range domain by correlation with a section of the surveillance signal that has at least a length of T_B. For each time shift (range cell) a Doppler FFT then is applied to n_B correlation outputs. The range profile update rate T_B is equal to the batch length and assumes the role of the T_{PRI} of conventional radar signal processing. Thus, the strong bond of the range-scope with the Doppler ambiguities still exists. However, the range-dependent correlation loss is not resolved in [13] beyond a single batch interval T_B.

In the following, it is presented how the strong interdependency of range-scope and Doppler-scope can be eliminated by utilizing the new RFB algorithm.

Resolving the range-Doppler bond by the RFB algorithm

The range profile update rate of the RFB algorithm is defined by the elementary matched filter length T_r. It allows Doppler processing with maximum unambiguous frequency $f_{d,u}$ of

$$|f_{d,u}| = \frac{1}{2T_r}. \tag{15}$$

For a set of P range profiles which is analyzed by a Doppler-FFT along each range cell, the frequency resolution is determined by the overall coherent processing interval $P \cdot T_r$ to

$$\Delta f_d = \frac{1}{PT_r}. \tag{16}$$

It is important to point out that the range extension factor M does not play any role for the Doppler analysis. This means the observable range scope R_{max} is independent of the resolution and ambiguity of the Doppler analysis when the RFB algorithm is applied.

For very short section length values of T_r, the number of coherently processed range profiles P significantly increases for a given coherent processing interval T_D. In case of simply Doppler analyzing this set of range profiles, the length of the FFT would linearly increase with the parameter P and the maximum unambiguous Doppler shift would increase to large values according to (15).

Tailoring the Doppler scope

The proposed procedure described in this section reduces the number of Doppler calculations by carefully adjusting the Doppler analysis parameters to the requirements of the particular radar application.

Figure 4 describes a Doppler processing optimized in terms of computational efficiency. The requirement for this procedure is that the number of coherently processed range profiles P can be factorized to integer values

$$P = N_\Sigma \cdot N_\mathcal{F}. \tag{17}$$

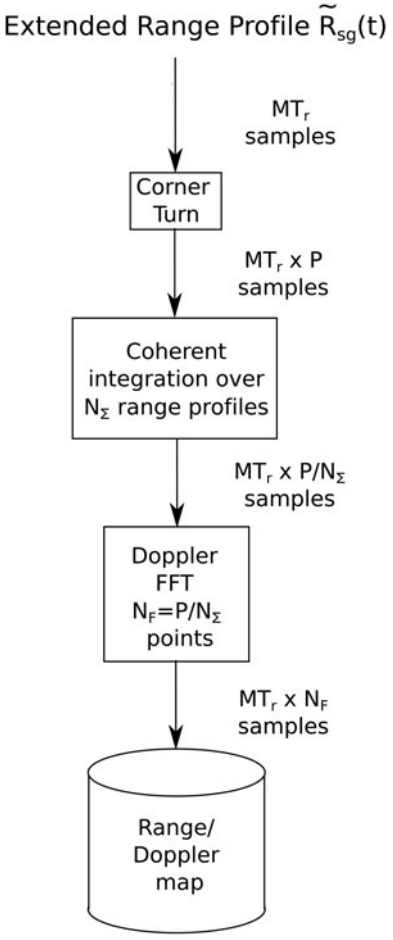


Fig. 4. Flow chart of Doppler scope adjustment while preserving the Doppler resolution. Coherent integration of range profiles prior to the Doppler FFT brings flexibility to the section length T_r of the RFB algorithm. The processing gain is not affected.

According to Fig. 4, the factor N_Σ describes the integer number of subsequent range profiles that are element-wise integrated prior to the FFT operation. After coherent range cell integration the frequency analysis is performed with a reduced number of FFT points equal to $N_\mathcal{F}$.

As the integration is performed coherently, the processing gain of the full analysis procedure does not change and so does the Doppler resolution

$$\Delta f_d = \frac{1}{T_r \cdot (N_\mathcal{F} \cdot N_\Sigma)}. \tag{18}$$

But the coherent range cell integration reduces the effective range profile update rate from $(1/(T_r))$ to $(1/(N_\Sigma \cdot T_r))$ which limits the maximum Doppler extent (Doppler scope) to

$$|f_{d,u}| = \frac{1}{2} \cdot \frac{1}{N_\Sigma \cdot T_r}. \tag{19}$$

By this procedure an FFT implementation with a length much shorter than the full number of range profiles P can be utilized as long as the resulting Doppler scope fits the requirements of the application. This fact significantly increases the computational efficiency of the Doppler analysis.

https://doi.org/10.1017/S175907871800171X Published online by Cambridge University Press



Fig. 5. Installation of the X-band noise radar demonstrator (50 MHz bandwidth, ERP < 2 W) in the field with two staring horn antennas mounted at a height of 3.5 m looking along a country road.

Practical considerations

The performance of the range–Doppler map resulting from the procedure presented in this paper can be adjusted by selecting the independent parameters N_Σ, M, and P appropriately, within the bounds of (7).

The section length T_r can be chosen first, based on technical implementation considerations.

For a given application, the range–Doppler performance of a noise radar system can be adjusted based on assumptions or *a priori* information on the expected targets as follows. It is assumed that the elementary matched filter operation is implemented with a fixed filter length T_r. This especially is the case for modern FPGA-based radar systems.

First, according to the application's maximum range of interest, the RFB parameter M is chosen, which represents the number of matched filters in the filter bank.

Second, the required processing gain based on the requested detection probability of a given target radar cross-section at a given distance defines the coherent processing interval. For a fixed section length T_r it only affects the value of P, i.e. the size of the set of range profiles.

Third and independent of M, the Doppler scope is considered by respecting the expected target velocity v_{max}. The parameter N_Σ is selected from the already chosen parameter P, the fixed value T_r and the velocity v_{max}.

Following this procedure, a well-tailored range–Doppler map is created by calculating range–Doppler combinations only in the given range and Doppler scopes of interest.

An extreme case of the presented algorithm can be applied to static scenarios, i.e. for $v_{max} = 0$ with $N_\mathcal{F} = 1$ and $N_\Sigma = P$. The full set of P output signals of the RFB then is coherently integrated forming a single range profile with extended range scope and full coherent processing gain. The computational effort is significantly reduced as compared with the direct correlation of surveillance and reference channels.

Experimental verification

This section presents a dedicated experimental test of the RFB algorithm. The scopes of both dimensions of the range–Doppler map have been strictly tailored to the given situation of the experiments.

Experimental set-up

An X-band noise radar demonstrator with a signal bandwidth of 50 MHz and <2 W effective radiated power (ERP) was available for the tests. This radar is implemented using the heterodyne receiver principle. The received echo signal (surveillance channel) and a copy of the transmitted signal (reference channel) are digitized and a digital implementation of the RFB generates range–Doppler maps based on a given set of parameters. The raw data are saved for verification.

During the experiment, staring antennas have been connected to the demonstrator and mounted on a tripod in 3.5 m height oriented along a country road.

On this road a car was driving cooperatively with velocities of over 100 km/h when approaching the radar and of about 50 km/h when departing from the radar.

The maximum available target distance was 250 m due to the shape of the particular road section. Figure 5 shows the installation of the radar demonstrator while the cooperative radar target is displayed in Fig. 6. This image is a still taken from a surveillance camera which was used for visual confirmation.

A Gaussian pseudo noise signal of 50 MHz bandwidth was used as radar waveform. Its period was equal to 200 ms, being much larger than the recording interval of the receiver. Thus, this waveform can safely be treated as a non-periodic signal from the data analysis point of view.

In this particular set-up, the motion of the target follows the line of sight of the radar. No significant tangential component of the motion does exist. A simple mapping of tachometer velocity of the car and measured velocity of the radar echo can be made.

For this reason, the radar data representation was converted from the Doppler shift of echo signals to target velocity values.

Experimental results

Two major results can be drawn from the analysis of data obtained by these experiments. The first result shows the validity of the RFB algorithm in terms of valid range measurement and also valid Doppler measurement. The second result supports the basic assumption that neither the velocity resolution nor the processing gain are affected by the different factorization values of (17).

Range and Doppler measurement verification

This section describes the results of the experiments regarding the creation of valid range–Doppler maps using the RFB algorithm. The implemented elementary correlation length was equivalent to $T_r = 700$ ns. With $M = 3$, the range scope of both displayed maps has been adjusted to 210 m, which covers most of the observed length of the country-road. The velocity analysis was adjusted to the maximum possible speed of the Audi A6 station wagon which is limited to 240 km/h in the respective configuration. The maximum available coherent processing interval in this recording was $T_{CPI} = 16$ ms. With the resulting velocity resolution of 3.6 km/h, a 128 point FFT was sufficient for analyzing the maximum expected Doppler of the target. Thus, from $T_{CPI} = PT_r = 16$ ms and (17) it follows that the choice of setting $N_\mathcal{F}$ to 128 results in $N_\Sigma = 15625$ coherent summations as the sampling frequency is equal to 125 MHz.

Figures 7 and 8 show the resulting range–Doppler maps that have been created by the RFB algorithm with the tailored scopes

https://doi.org/10.1017/S175907871800171X Published online by Cambridge University Press



Fig. 6. Station wagon used as cooperative moving radar target driving along a country road with speeds of 50 km/h in one experiment and more than 100 km/h in a second experiment.

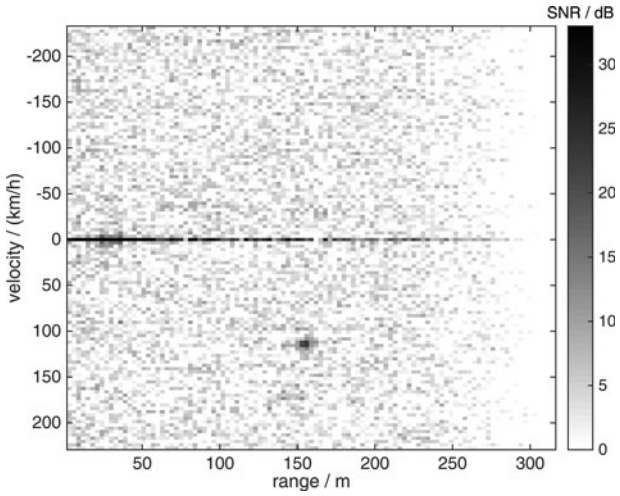


Fig. 7. Measured range-velocity map of a car approaching with 115 km/h was created by the RFB algorithm. The Doppler dimension was converted to relative speed for verification purposes. The signal to noise ratio of the target is higher than 25 dB in this figure.

in both dimensions. The moving target can be clearly identified in both figures with an SNR of more than 25 dB. In Fig. 7 the distance between radar and car is determined to 156 m and the measured velocity of the car is 115 km/h. While the car was on its way back to the starting point of the track with much slower speed, the recording of Fig. 8 was made showing 50 km/h radial velocity and a distance of 132 m.

No clutter suppression or weighting was applied to the data as the pure output of the basic RFB algorithm is to be demonstrated in this section. Due to the wide beam of the horn antennas, and lack of clutter suppression, clutter is well visible at zero Doppler.

Doppler scope tailoring verification

The procedure described in Fig. 4 assumes that the coherent processing gain and the velocity resolution of the data analysis is unaffected by the choice of $N_\Sigma N_\mathcal{F}$-factorization if the requirements of the observed scene are respected.

To underline this assumption, the same samples of the experiment displayed in Fig. 7 have been processed with different RFB parameter configurations. Figure 9 shows the results of this

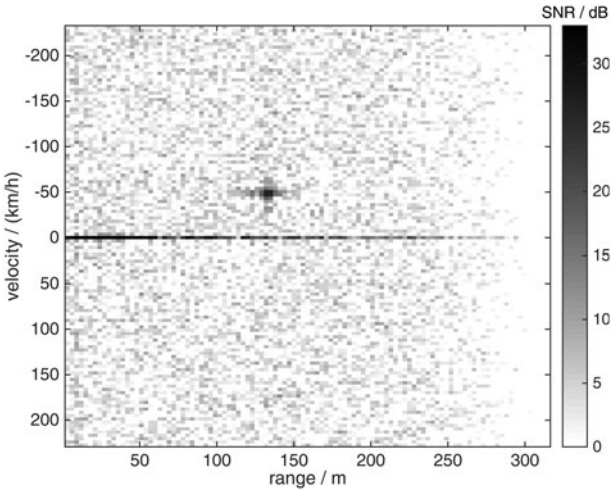


Fig. 8. The movement of the car driving in the opposite direction with lower speed of 50 km/h was also detected and correctly measured by the RFB algorithm.

investigation. The plots are labeled referring to the parameter $N_\mathcal{F} = (P/(N_\Sigma))$ which is more intuitive than N_Σ.

It can be clearly seen in Fig. 9 that the velocity resolution is constant for the exemplary combinations and that for all configurations the target peak of the moving target at 115 km/h is processed with full coherent processing gain. Minor differences in the Doppler side lobes can be observed for higher velocity values. Close to velocity value zero the curves perfectly match.

Discussion

The RFB algorithm can be verified by direct comparison of its results to those of the CAF. Figure 10 displays the result of a conventional CAF computation. The image is a cutout of the range-velocity matrix covering the range scope from 0 to 250 m and the huge velocity scope of $|v| < 1.4 \cdot 10^6$ km/h.

It is important to note that the more efficient RFB algorithm delivers the same target values as the conventional CAF as can be seen by comparing the results shown in Figs 7 and 10. The main difference between both figures can be observed at ranges beyond the Range scope of interest being 210 m. A fading effect is visible in the RFB according to Fig. 3. Obviously this effect is not present in the results created by solving the CAF.

The results of the experiments show that the RFB algorithm offers valid measurements of distance and velocity. In [4] it was demonstrated how much more efficient the RFB is compared to the CAF based on a generalized investigation of the computational cost of these algorithms. Furthermore, in the present work the computational cost of the RFB implementation was improved by tailored Doppler processing.

For efficiency purposes, the coherent processing of P adjacent range profiles, which can be factorized into a linear combination part and a frequency analysis part, should include as many linear combinations of range profiles as the resolution and range/Doppler ROIs allow.

It was taken into account that according to [15] the cost for an FFT of length $N_\mathcal{F}$ can be rated by

$$\mathcal{O}\left(N_\mathcal{F} \log_2(N_\mathcal{F})\right) \tag{20}$$

https://doi.org/10.1017/S175907871800171X Published online by Cambridge University Press

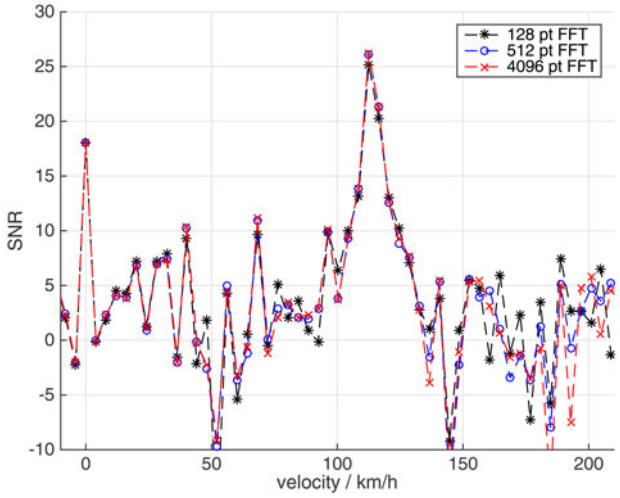


Fig. 9. A vertical cut of the range-velocity map of Fig. 7 at the range position of the moving target. The results of different variations of $N_{\mathcal{F}}$ with exemplary values from 128 to 4096 FFT points are shown. The peak of the coherently processed target remains constant for all variations of the FFT length $N_{\mathcal{F}}$ while the coherent processing gain is preserved according to the algorithm displayed in Fig. 4.

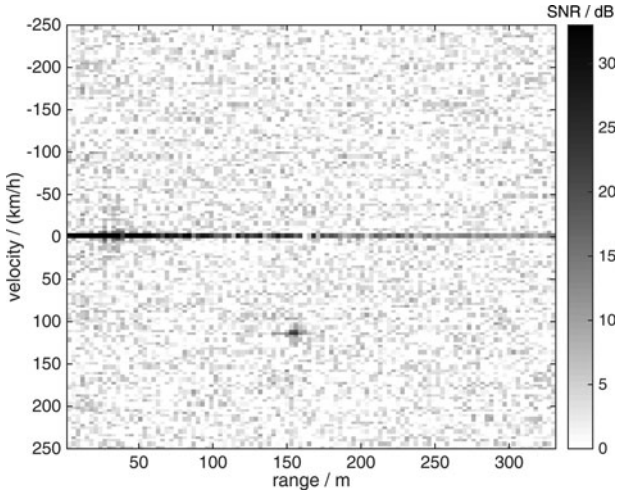


Fig. 10. The same data as in Fig. 7 but computed by solving the Cross Ambiguity Function. The illustrated image is a zoom into the full CAF covering velocity values of ± 1.4 million km/h.

elementary operations whereas the cost for a coherent summation of N_Σ samples is linear with cost of

$$\mathcal{O}(N_\Sigma). \tag{21}$$

The relative cost of different factorizations thus can be rated with (22) and (21) to

$$\mathcal{O}\left(\frac{N_{\Sigma_1} N_{\mathcal{F}_1} \log_2(N_{\mathcal{F}_1})}{N_{\Sigma_2} N_{\mathcal{F}_2} \log_2(N_{\mathcal{F}_2})}\right) = \mathcal{O}\left(\frac{\log_2(N_{\mathcal{F}_1})}{\log_2(N_{\mathcal{F}_2})}\right) \tag{22}$$

for any valid factorization $N_{\Sigma_1} N_{\mathcal{F}_1} = N_{\Sigma_2} N_{\mathcal{F}_2} = P$.

The experimental results of Fig. 9 show matching results for the respective velocity scope of the analysis for different linear combination to frequency analysis factorizations. For $N_{\mathcal{F}} = 128$ the maximum displayed velocity is 230 km/h whereas for $N_{\mathcal{F}} = 4096$ it is equal to more than 8000 km/h which is unnecessarily high for the configuration in the experiment.

The computational speed up between both extreme cases is equal to 42% by reducing the FFT length from $N_{\mathcal{F}_2} = 4096$ to $N_{\mathcal{F}_1} = 128$. The data rate of the RFB output matrix is reduced to 3%.

Conclusions and outlook

In this paper, a customizable and efficient range–Doppler processing algorithm was presented. The intense use of short Fast Fourier Transforms results in an improved efficiency compared with calculating range–Doppler maps by solving the CAF, which usually is referred to in noise radar technology.

Range-dependent correlation losses have been resolved and the bond of range scope with Doppler scope has been cut.

The described procedure is based only on parameter variations that apply to the received signals. The performance of the range–Doppler processing can be chosen without altering the transmitted signal. In future, even several different RFB implementations with different sets of parameters might be executed in parallel on the same sample of received data, each of them fulfilling different tasks. The RFB is also compatible with a varying section length parameter T_r, like in the conventional *staggered PRF* surveillance radars, to enhance the available RVP.

The presented approach paves the way toward real-time implementation of range–Doppler computations in CE noise radar signal processing.

References

1 **Thayaparan T *et al.*** (2008) Mutual interference and low probability of interception capabilities of noise radar. *IET Radar, Sonar & Navigation* **2**, 294–305.
2 **Galati G, Pavan G and De Palo F** (2016) Compatibility problems related with pulse-compression, solid state marine radars. *IET Radar, Sonar & Navigation* **10**, 791–797.
3 **Pace PE** (2009) *Detecting and Classifying Low Probability of Intercept Radar*. Boston: Artech House.
4 **Wasserzier C and Galati G** (2018) Advanced range-Doppler processing in noise radar, 22nd International Microwave and Radar Conference (MIKON), pp. 464–467.
5 **Poullin D** (2005) Passive detection using digital broadcasters (DAB, DVB) with COFDM modulation. *IEE Proceedings - Radar, Sonar and Navigation* **152**, 143–152.
6 **Sturm C *et al.*** (2013) Spectrally interleaved multi-carrier signals for radar network applications and multi-input multi-output radar. *IET Radar, Sonar & Navigation* **7**, 261–269.
7 **Woodward PM** (1953) *Probability and Information Theory with Applications to Radar*. London: Pergamon Press Ltd.
8 **Levanon N and Mozeson E** (2004) *Radar Signals*. Hoboken, NJ: John Wiley & Sons.
9 **Richards MA *et al.*** (2010) *Principles of Modern Radar*. Edison, NJ: Scitech publishing.
10 **Kulpa K** (2013) *Signal Processing in Noise Waveform Radar*. Boston: Artech House.
11 **Malanowski M and Kulpa K** (2012) Detection of moving targets with continuous-wave noise radar: theory and measurements. *IEEE Transactions on Geoscience and Remote Sensing* **50**, 3502–3509.
12 **Min WK *et al.*** **Numerical and experimental verifications of digital correlator model for random noise radar. IEEE Antennas and Propagation Society International Symposium, Charleston, June 2009.**

https://doi.org/10.1017/S175907871800171X Published online by Cambridge University Press

13 **Moscardini C *et al.*** (2015) Batches algorithm for passive radar: a theoretical analysis. *IEEE Transactions on Aerospace and Electronic Systems* **51**, 1475–1487.
14 **Papoulis A** (1977) *Signal Analysis*. New York: McGraw Hill.
15 **Dongards J and Sullivan F** (2000) Guest editors' introduction to the top 10 algorithms. *Computing in Science & Engineering* **2**, 22–23.



Christoph Wasserzier received a degree in Electrical Engineering and Information Technology from the RWTH Aachen University in 2009. He is a research scientist at Fraunhofer FHR since 2009 and his main research interests are LPI and LPE radars from many different aspects.



Gaspare GALATI received the Dr. Ing. Degree (Laurea) in Nuclear Engineering in 1970. From 1970 till 1986 he was with the company Selenia (Finmeccanica group) where he was involved in radar systems analysis and design and, from 1984 to 1986, headed the System Analysis Group. From March, 1986 he was an associate professor at the Tor Vergata University of Rome; from November 1996 to 2017 he was a full professor of Radar Theory and Techniques at the Tor Vergata University. In 2017, he has been designated Honorary Professor by the Ministry of Education. His main interests are in radar theory and techniques, detection and estimation, noise radar, navigation and air traffic management. He is the author/coauthor of about 300 papers, 20 patents, and 10 books on those topics.

https://doi.org/10.1017/S175907871800171X Published online by Cambridge University Press